Chapter 5

Mathematical Modeling of Isothermal Drying and its Potential Application in the Design of the Industrial Drying Regimes of Clay Products

Miloš Vasić, Zagorka Radojević and Robert Rekecki

Additional information is available at the end of the chapter

http://dx.doi.org/10.5772/64983

Abstract

The processes of simultaneous moisture and heat transfer, which are often nonstationary, and the distinct nature and properties of the material to be dried complicate the description of the drying process. The theory of moisture migration and modeling of drying process has been the subject of many studies. Three theories, the diffusion, the capillary flow, and the evaporation-condensation, have won general recognition for the explanation of moisture transfer in porous media. This study has several objectives. The first one was to present a new method for calculation of the variable effective diffusivity as well as to identify different drying mechanisms and its exact transitions during isothermal drying of clay tiles. The second and main objectives were to analyze all obtained isothermal data, to create a link with the comprehensive theory of moisture migration during drying, and to set up the non-isothermal drying process. The procedure was based on the principle of controlling the mass transport during the drying process. Proposed regimes were consisted from several isothermal segments. Isothermal segments were selected and specificated in accordance with the clay raw material nature and the moisture migration theory.

Keywords: drying regime, effective diffusivity, clay tile, non-isothermal drying, shrinking

1. Introduction

Drying represents very important and complex process in the production of clay tiles, which involves simultaneous heat and mass transfer between the body and the surrounding atmosphere. The whole process consists of several periods characterized with different mechanisms of internal moisture transfer. Until recently, three theories, the diffusion theory, the capillary flow theory, and the "evaporation-condensation theory," have won general recognition for an explanation of moisture transfer in porous media. During drying, several mechanisms are controlling the overall internal moisture transport from the drying material up to its surface. In order to describe the complete internal transport with the same equations as pure diffusion and to take the correction for all secondary types of mass transfer into account, it is suitable to simply replace the pure diffusion coefficient with an effective diffusion coefficient. This procedure was successfully applied in the reference [1]. Within the same reference, it is stated that "the effective moisture diffusivity represents an overall mass transport property of moisture which includes molecular diffusion, the Knudsen diffusion, the non-Fickian or stress-driven diffusion, capillary motions, liquid diffusion through solid pores, vapor diffusion in air-filled pores, vaporization-condensation sequence flow, and hydrodynamic flow mass transfer mechanisms."

Determination of the effective diffusion coefficient is essential for a credible description of the mass transfer process, described by Fick's equation [2]. Description and modeling of drying process based on the calculation of constant effective moisture diffusivity have been the subject of many studies [3–7]. The plot of effective moisture diffusivity vs. time or moisture content (Deff-t or Deff-MR curve) is a good indicator to evaluate and present an overall mass transport property of moisture during isothermal drying. Determination of time-dependent effective moisture diffusivity along with the detection of Deff-MR curves has been reported in several studies [8–11]. The facts that capillary flow is a predominant mechanism within the constant drying period while, in the falling drying period, the evaporation-condensation and vapor diffusion are the predominant mechanisms, have won general recognition for the explanation of moisture transfer in porous media. The comprehensive theory of moisture migration during drying which represents a method useful to trace and quantify all possible mechanisms of moisture transport and their transitions during the isothermal drying process was recently reported [12].

This study has several objectives. The first one was to shortly present the theory of moisture migration along with the method for calculation of the variable effective diffusivity. The next one was to calculate the variable effective diffusivity, to divide drying curve in segments, and to identify all possible mechanisms of moisture transport within a clay roofing tile for several different experiments, in which drying air parameters were constant. The main objectives of this study were to analyze all obtained isothermal data, to create a link with the nature of the raw clay material and the comprehensive theory of moisture migration during drying, and finally to design the non-isothermal industrial drying regime.

2. Methods and materials

After using appropriate initial and boundary conditions, along with reasonable assumptions, Cranck has presented the analytical solution of Fick's second diffusion law for several standard

http://dx.doi.org/10.5772/64983

geometries, such as tile, cylinder, and sphere [13]. Hence, on the base of the lumping approximation, which assumes that the effective diffusivity is an overall mass transport property, the Cranck solution for tile geometry can be expressed as Eq. (1):

$$MR = \frac{X - X_{eq}}{X_0 - X_{eq}} = \frac{8}{\pi^2}\sum_{n=1}^{\infty}\frac{1}{(2n+1)^2} exp\left(\frac{-(2n+1)^2}{4}\right)\pi^2 \frac{D_{eff}t}{l^2} \tag{1}$$

In order to estimate effective diffusivity from Eq. (1), many researchers were using a simplifying method [14, 15]. They assumed that for sufficiently long drying times, the terms in the infinite summation series in Eq. (1) converge rapidly and in most cases may be accurately approximated by the first term of the series. This method is commonly known as "simplified slope" model. Two programs for determination of effective diffusion coefficient, based on mathematical calculation of Fick's second law and the Cranck diffusion equation, were recently presented for clay tiles [2, 6, 7].

2.1. Method for estimation of the time-dependent effective diffusivity

Zagrouba was one of the first researchers that had reported the "slope" method as a possible solution for estimation of the dependent effective diffusivity at various moisture contents for clay materials [11]. The Fourier diffusion number (F_0) has to be calculated from Eq. (2), while constant diffusion coefficient D_0 is obtained from the "simplified slope" method. The dependent effective diffusivity D_{eff} is calculated from Eq. (3). This method has been widely applied in several studies such as [8, 9, 16]:

$$F_0 = \frac{D_0 t}{l_0^2} \tag{2}$$

$$D_{eff} = \frac{\left(\frac{\partial MR}{\partial t}\right)_{exp}}{\left(\frac{\partial MR}{\partial F_0}\right)_{th}} l_0^2 \tag{3}$$

2.1.1. Modified slope method

Better and more accurate solution, called "modified slope" method, for calculation and estimation of time-dependent effective diffusivity based on the "slope" method was presented [12] and recently applied in two studies [17, 18]. The essence of this new model is reflected in replacing the constant term l_0 in Eqs. (2) and (3) with an interchangeable $l_{(t)}$ term and by using the model that includes shrinkage, which is presented in the study [7], for calculation of the constant diffusion coefficient D_0. Interchangeable $l_{(t)}$ term must be registered experimentally. The final calculation formula is presented in the form of Eq. (4):

$$D_{eff_{(t)}} = \frac{\left(\dfrac{\partial MR}{\partial t}\right)_{exp}}{\left(\dfrac{\partial MR}{\partial F_0}\right)_{th}} l_{(t)}^2 \tag{4}$$

2.1.2. Moisture migration theory

Typical curves, which represent the dependence of the effective moisture diffusivity as a function of the moisture content or drying time obtained using calculation method presented in the study [12], are presented in **Figure 1**.

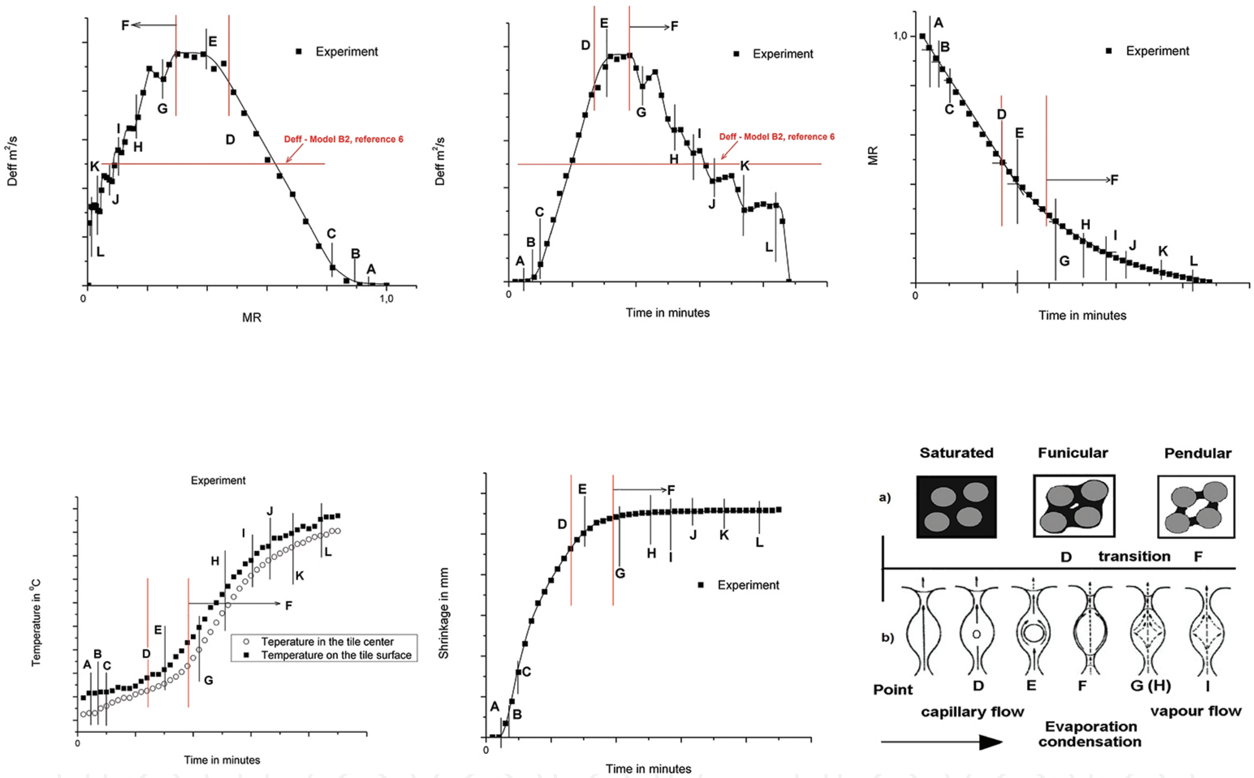

Figure 1. Typical time-dependent effective moisture diffusivity curves (Deff-MR and Deff-t).

It is important to highlight the significance of the characteristic pattern shown in **Figure 1**. It indicates all possible mechanisms of moisture transport along with their transitions from one to another during the constant and the falling drying period for isothermal experiments.

At the beginning of the drying process, effective moisture diffusivity values are equal to zero until characteristic point A is reached. This drying period is commonly known as the "initial heating segment." It is a relatively short period. The quantity of evaporated water is small, and shrinkage of the green body (clay tile) is not detected. The clay tile surface is heating up from its starting temperature up to the wet-bulb temperature. Moisture diffusivity values are practically zero suggesting that the overall mass transport is negligible.

After the initial heating period is over, the effective moisture diffusivity values are increasing as the moisture ratio is decreased, until characteristic point E is reached. This period is commonly known as the "constant drying rate period." Throughout this period, the surface of the green body is constantly covered with a continuous film of water. The surface temperature is constant and has a value corresponding to the wet-bulb temperature of the air. The shrinkage of the green body is characteristic for this drying period. The end of the constant rate period is marked by a maximum in capillary pressure. Cracking of the green body is most likely to occur at this point of the drying process [19–21].

From point A to point B, liquid is transporting through the biggest capillaries. This transport is caused by a gradient of the capillary potential and is commonly known as the "capillary pumping flow." Throughout this period, the quantity of evaporated water and detected sample shrinkage is relatively small. The "hydrodynamic flow" (caused by viscosity) is negligible and that the overall mass transport is governed only by capillary pumping flow mechanisms.

From point B up to point D, liquid is transported simultaneously by two mechanisms. The main mechanism is capillary pumping flow, caused by the gradient of the capillary potential originating from still saturated capillaries, and the second one is hydrodynamic liquid flow in pores, which arises from the difference in total pressure caused by friction. Capillary pumping flow up to point C was caused by the still present macro capillaries, while the same flow up to point D was caused by the presence of mezzo capillaries. Throughout this period, the quantity of evaporated water and detected sample shrinkage is considerably higher than in the already presented drying segments. Point D is commonly known as the "upper critical point" which is indicating the beginning of the transition from the "funicular" to the "pendular" state. It is important to highlight that in the "funicular" state, continuous threads of moisture are present in the pores, while in the "pendular" state this is not the case. From this point on, the clay tile surface is not fully covered by a water film. "Dry" patches will appear on the surface for the first time. The drying front is starting to recede.

From point D up to point E, liquid and vapor are transported simultaneously. Liquid is transported by three mechanisms. The main one is capillary pumping flow. Capillaries in the funicular state are generating the pressure gradient which secures the capillary pumping flow. The difference in total pressure caused by friction provides hydrodynamic liquid flow in pores which represents the second transport mechanisms. The concentration gradient of the liquid in the pores is the driving force for the liquid diffusion which represents the third transport mechanisms. The difference in total pressure caused by friction secures the hydrodynamic vapor flow in pores. Deviation from a constant drying rate is first registered as point E, which is commonly named the "critical" point. A partially wet surface is able to provide a constant or a falling drying period depending on the fraction of wet surface and the boundary layer thickness. The influence of a partially wet surface on the transition from a constant rate to a falling rate of drying is described in the study [22].

From point E up to point F, the fraction of the wet surface is decreased until the "last" wet patches disappeared from the surface. This point is commonly known as the "lower" critical point which indicates the end of the transition from the "funicular" to the "pendular" state. In other words, the moisture content is decreased, and the gas bubbles attained the dimensions of the pores, breaking the continuous threads of moisture in the pores. Moisture is transported up to the surface by creeping along the capillary when the liquid is in the funicular state or by the successive evaporation-condensation mechanism between liquid bridges. When the "pendular" state is reached, there is no further contraction of the drying body, and consequently the possibility of the drying body to crack is extremely small.

During the drying process, the temperature increase is registered. The temperature is increasing slowly from point D up to point E, and then moderate temperature increase is registered up to point F. After point F is reached, the temperature of the system is rising rapidly up to point I. From point I up to point K, the temperature is rising very slow and is practically close to the level off at the so-called pseudo-wet-bulb temperature. The temperature is increasing again just before the end of the drying process until it reached the level of the final temperature.

With further drying from point F to point G, the moisture is transported up to the surface by the successive evaporation-condensation mechanism between liquid bridges. Simultaneously with the evaporation and condensation mechanisms, liquid starts to evaporate within the pore space at a growing rate, causing the vapor pressure to increase. These two mechanisms move the "pendular" water up to the surface.

The G–H segment is consisted from two parts. Locally produced vapor is accumulating within the pores causing a local increase in the effective diffusivity within the first G–H segment. In one moment, the local vapor pressure is exceeding the critical value, and the vapor is practically "blown" away up to the surface. During the vapor release, some liquid bridges of "pendular" water are also transported. This kind of moisture transport is accompanied with the local decrease of the effective diffusivity value which is characteristic for the second G–H segment. The movement of the remaining "pendular" water in the H–I segment is mostly caused by the vapor pressure existing within the pore space.

After "pendular" water is removed, the evaporation occurs only inside the body, and the temperature of the surface approaches the so-called pseudo-wet-bulb temperature, and at the end of the drying, it reaches ambient temperature. This I–L segment is commonly known as the "diffusion period." It is divided into three parts. The first one "I–J" represents pure molecular diffusion, while the second "J–K" and third "K–L" ones represent, respectively, transitional and the Knudsen diffusion.

2.2. Experimental

The raw material, used in this study, was obtained from the largest roofing tile manufacturer in Serbia. "Kanjiza's" clay raw deposit is formed from two layers. The first layer is commonly known as the "yellow clay." It contains a relatively small amount of clay minerals (under 23 wt.%), but it is rich in quartz, carbonates (above 20 wt.%), and feldspar minerals. The second layer commonly known as the "blue clay" predominantly contains clay minerals: illite, smectite, chlorite, and kaolinite. The industrial raw material mixture and the one used in this study consist, respectively, 80 and 20 wt.% of blue and yellow clay [23].

Initial characterization of Initial characterization of the raw material has included determination of particle size distribution (PSD) analysis, standard silicate chemical analysis (SSA), qualitative and semiquantitative XRD analysis, and TGA (TG analysis). Standardized procedures, described, respectively, in SRPS U.B1.018:2005 and SRPS B.D8.210:1982 norms, were used for PSD and SSA determination. Qualitative and semiquantitative XRD analysis and TGA (TG analysis) were reported in the study [24].

After initial characterization, the raw material was homogenized and prepared for the forming process. During the homogenization process, the raw material was moisturized and milled using laboratory differential mills.

Laboratory roofing tile samples 120 × 50 × 14 mm were formed in a laboratory extruder "Hendle" type 4, under a vacuum of 0.8 bar. Formed samples were packed into plastic bags which were afterward sealed and put into a glass container with lid. Glass containers with samples were kept in the air-conditioned room in which temperature and relative humidity were maintained, respectively, at 25°C and 65%. This procedure allows the minimal moisture content fluctuations within the stored samples.

Series of isothermal drying curves was recorded. Laboratory recirculation dryer in which drying parameters (humidity, temperature, and velocity) could be programmed, controlled, and monitored was used. Regulation of wet air parameters within the range of 0–125°C, 20–100%, and 0–3.5 m/s with accuracies of ±0.2°C, ±0.2%, and ±0.1% for temperature, humidity, and velocity, respectively, was limited by the laboratory dryer design. The mass of the samples and their linear shrinkage were continually monitored and recorded during the experiments. The accuracies of these measurements were 0.01 g and 0.2 mm, respectively. Experimental conditions presented in **Table 1** were used in the present study. Each experiment was repeated two times.

Experiment	Group	Air humidity, V/%	Air temperature, T/°C
1	I	80	35
2	I	80	40
3	II	70	40
4	II	70	45
5	III	60	40
6	III	60	45

Table 1. Experimental conditions.

The modified slope method was used to calculate the functional dependence of the effective diffusivity vs. moisture content (Deff-MR), to divide obtained curves in segments, and to identify all possible mechanisms of moisture transport within each drying segment. Roofing tile samples were afterward dried to constant mass. Dried samples were heated in oxygen atmosphere with the heating rate of 1.4°C/min from room temperature up to 610°C and further with the heating rate of 2.5°C/min up to the 1000°C. Samples were kept at 1000°C for 2 hours. Flexural strength was determined on dried (DSFS) and fired samples (FSFS) using the procedure described in EN 538 norm.

Obtained data were analyzed and used to set up several non-isothermal drying regimes. Drying air parameters which were maintained in each proposed drying regime are presented in **Table 2**. Duration of the approximately isothermal drying segments was detected from the isothermal curves Deff-MR. Tiles were then dried to constant mass and fired using the same heating rate as one previously mentioned. DSFS and FSFS were determined. Twist coefficient (TWC) and longitudinal camber (LOC) coefficient and transverse camber (TRC) coefficient were determined on fired samples using the procedure described in EN 1024 norm.

Experiment	Segment				
	I	II	III	IV	V
7	Exp. 1	Exp. 2	Exp. 3	Exp. 4	70°C/40%
8	Exp. 2	Exp. 3	Exp. 5	Exp. 6	70°C/40%

Table 2. Experimental conditions—proposed drying regimes.

3. Results and discussion

Results of several analyses, used for initial characterization of the raw material, are presented in **Table 3**. The mass content of SiO_2, Al_2O_3, CaO, and MgO obtained by SSA analyses is indicating the presence of free quartz, feldspars, clay minerals, and carbonate minerals in the analyzed raw material. Results of qualitative mineralogical and XRD analyses, reported in the study [24], have confirmed the presence of quartz, feldspars (orthoclase), illite, muscovite, kaolinite, montmorillonite, chlorite, calcite, and dolomite in the analyzed raw material. Semiquantitative XRD mineralogical analysis has quantified the presence of previously mentioned minerals. The mass content of clay, silt, and sand obtained by PSD analyses is indicating that the analyzed raw material is classified as clay loam suitable for clay roofing tile production.

All possible mechanisms of moisture transport and their transition from one to another during drying for isothermal experiments are identified and are shown in **Figure 2**.

http://dx.doi.org/10.5772/64983

Chemical composition in wt%		Mineralogical composition in wt%	
Loss on ignition 1000°C	6.24	Quartz	29
SiO_2	55.30	Feldspars (orthoclase)	17
Al_2O_3	16.00	Illite and muscovite	16
Fe_2O_3	6.12	Kaolinite	6
CaO	7.50	Montmorillonite	5
MgO	3.59	Chlorite	6
SO_3	0.00	Calcite	7
S^{2-}	0.00	Dolomite	6
Na_2O	1.10	Particle size composition in wt%	
K_2O	3.52	Clay (<2 μm)	46.2
MnO	0.08	Silt (2–20 μm)	29
TiO_2	0.54	Sand (>20 μ m)	24.2

Table 3. Initial characterization of the raw material.

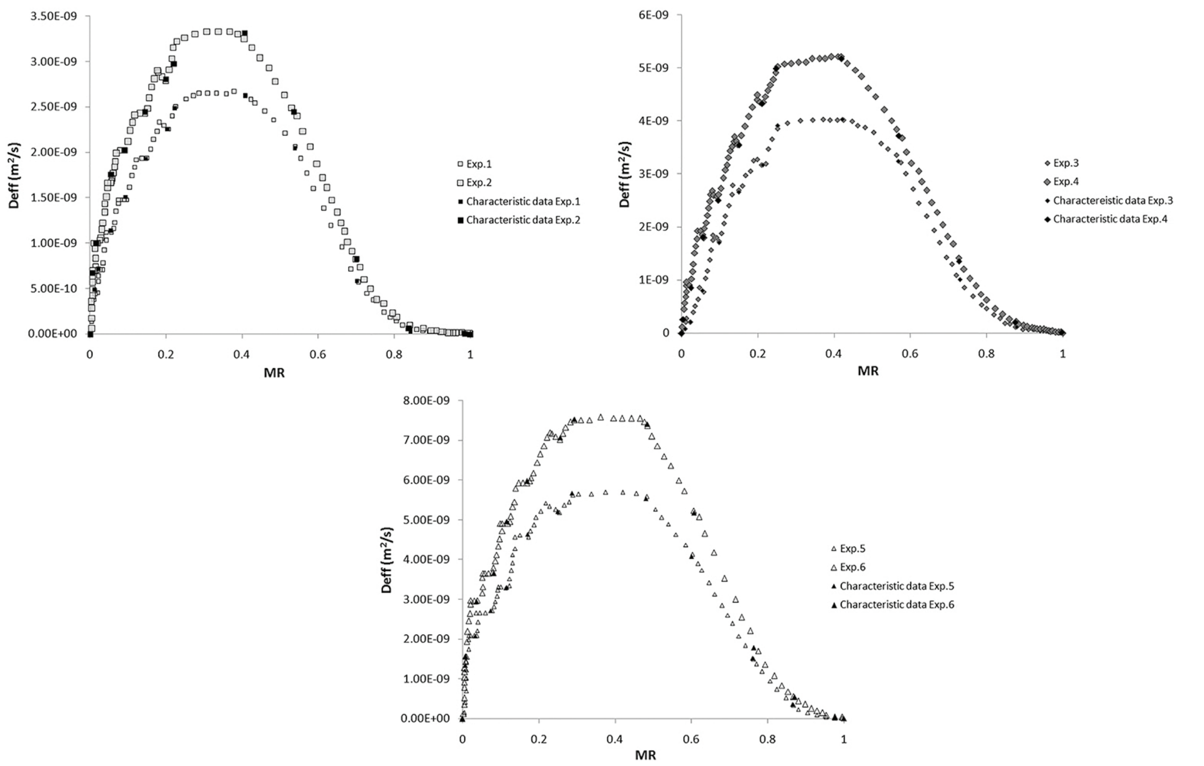

Figure 2. Estimated Deff-MR curves for isothermal experiments.

The procedure for setting up the non-isothermal drying regime that is consistent with the theory of moisture migration during drying was based on the principle of controlling the mass transport during the drying process and has demanded to divide the drying process into five segments. In each of these segments, approximately isothermal drying conditions were maintained (see **Table 2**).

The main functions of the first segment are to restrain the moisture transport (evaporation), through the boundary layer between material surface and the bulk air, and to heat the ceramic body to the temperature of the drying air. That is the reason why high values of the drying air humidity in the first segment were selected. In order to fulfill previously mentioned requirements, this drying segment is over when characteristic point C is reached. During the second drying segment, external transport (surface evaporation) and internal transport (of liquid water from the ceramic body up to the surface) have to be increased and simultaneously harmonized in such a way that the drying surface remains fully covered by a water film. That is the reason why in most cases drying air humidity in this segment is reduced. Its absolute value is still relatively high. This will increase the evaporation driving force and consequently will speed up the drying process. Drying air temperature in this segment may slightly increase compared to the previous segment. This will moderately increase the capillary transport as well as the drying rate. The second segment starts and ends when characteristic points C and D ("upper critical point") are, respectively, reached.

The third and fourth segment represents together a transitional drying period in which the sample is gradually shifting from "funicular" to "pendular" state. A higher fraction of wet surface and a thicker boundary layer produce and favor a constant drying rate period, while a smaller fraction of the surface and a thinner boundary layer shell favor and produce a falling drying rate. The main function of the third segment is to provide the conditions that will lead to the fact that partially wet surfaces provide a constant rate of drying. That is the reason why the humidity and temperature of the drying air within the third segment have to be carefully selected. Further reduction of the drying air humidity (see **Table 2**) will increase the evaporation driving force (external surface evaporation) and consequently will speed up the drying process. Drying air temperature in this segment may slightly increase compared to the previous segment. This will increase the capillary transport as well as the drying rate. The third segment starts and ends when characteristic points D and E are, respectively, reached.

Within the fourth segment, the fraction of the wet surface decreased until the "last" wet patches disappeared from the surface. At the end of the fourth segment, the system had reached the "pendular" state, and there is no further contraction of the drying body. The main function of this segment is to simultaneously harmonize the liquid transport originating from the pores which are near or just below the "dry" patches on the surface and are still in the funicular state with the liquid flow originating from the surface "wet" patches. That is the reason why drying air humidity in this segment is not reduced (see **Table 2**).

Further increase of the drying air temperature has a positive influence which has led to the liquid transport enhancement. The fourth segment starts and ends when characteristic points E and F ("lower critical point") are, respectively, reached. The main function of the fifth segment is to maximally facilitate the internal moisture transport up to the surface. That is the reason why drying air humidity in the fifth segment is further reduced, while drying air temperature is maximally increased [25].

Characteristic data for isothermal experiments from point A up to point F are presented in **Table 4**.

Exp.		**1**	**2**	**3**	**4**	**5**	**6**
Time (min)	A	58	51	49	36	23	21
	B	161	148	109	89	49	45
	C	280	253	190	170	82	75
	D	424	387	284	268	145	133
	E	526	484	360	338	187	170
	F	769	700	518	491	291	268
	TDT	1420	1250	1190	1050	730	625
	TDT—total drying time						

Table 4. Characteristic data for isothermal experiments from point A up to point F.

Duration of the approximately isothermal drying segments was not specified by experience or by trial-and-error method. It was detected from the appropriate isothermal Deff–MR curves (see **Figure 1** and **Table 4**). General procedure will be explained on experiment 7. Duration of the first segment was the same as the duration of the drying process in the case of experiment 1 from the beginning up to the characteristic point C. Duration of the second segment was the same as the duration of the drying process in the case of experiment 2 from the characteristic point C up to the characteristic point D. Duration of the third segment was the same as the duration of the drying process in the case of experiment 3 from the characteristic point D up to the characteristic point E. Duration of the fourth segment was the same as the duration of the drying process in the case of experiment 4 from the characteristic point E up to the characteristic point F. Duration of the fifth segment was limited to 90 minutes. This procedure was used to specify the duration of drying segments in each proposed drying regime. Calculated results are presented in **Table 5**.

Drying segment	**Segment duration *t* (min)**	
	Exp. 7	**Exp. 8**
1	280	253
2	134	94
3	76	42
4	153	98
5	90	90
TDT	733	577

Table 5. Calculated segment duration within proposed drying regimes.

It is important to define the minimum requirements for dried clay roofing tile which if satisfactory will ensure that the product is able to perform its function. In other words, dried clay roofing tiles has to be dried without cracks. Minimal flexural strength of dried and fired samples has to be, respectively, at least 0.73 and 1.2 kN (see EN 1304 norm). The mean value of the twist coefficient (TWC) and the mean value of the longitudinal camber (LOC) and transverse camber (TRC) coefficients calculated as described in EN 1024 norm shall comply, respectively, with the requirements stated in **Tables 1–3** presented within the EN 1304 norm. Proposed drying regimes were tested. Clay roofing tiles were dried without cracks. Flexural strength of dried and fired clay tiles (DSFS and FSFS) are presented in **Table 6**.

Experiment	DSFS (kN)	1000^0C
		FSFS (kN)
1	0.99	2.73
2	0.97	2.65
3	0.92	2.67
4	0.82	2.65
5	0.80	2.12
6	0.75	2.08
7	0.93	2.65
8	0.81	2.42

Table 6. Mechanical properties of dried and fired samples.

Experiment	Twist coefficient	Cambers R (%)	
	C (%)	Longitudinal	Longitudinal
1	0.29	0.33	0.33
2	0.45	0.50	0.50
3	0.90	0.68	0.68
4	1.23	0.87	0.87
5	0.72	0.79	0.79
6	1.18	1.05	1.05
7	0.48	0.51	0.51
8	0.71	0.69	0.69

Table 7. Twist and camber coefficients.

The mean TWC value and the mean LOC and TRC values for isothermal and non-isothermal drying regimes are presented in **Table 7**. Detailed analysis of data presented in **Table 7** has revealed that mean TC, RL, and RT is increasing with the increase of the drying air temperature as well as that under the same drying air temperature, TWC, LOC, and TRC values, presented in different experimental groups, is also increasing with the decrease of air relative humidity (see **Tables 1** and **7**). Maximally allowed deviation for TWC, LOC, and TRC is 2%. This criterion is defined in **Tables 1–3** of the EN 1304 standard.

TWC, LOC, and TRC values can be used as a good indirect indicator of the stress generation. In other words, higher TWC, LOC, and TRC values are correlated with the higher stress generation. The drying air with higher temperature and lower relative humidity leads to more rapid generation of the stress in the samples during drying which will result with the lower shape regularity (higher coefficients) and lower mechanical properties of the dried samples.

The shortest total drying time (TDT) for isothermal and non-isothermal drying regimes was, respectively, registered in experiments 8 and 6 (see **Tables 4** and **5**). The difference between TDT values related to previously mentioned experiments is relatively small. The lowest DSFS and FSFS values along with the highest mean TWC, LOC, and TRC values for non-isothermal drying regimes were registered in experiment 8. It is important to point out that dried and fired clay roofing tiles in each proposed non-isothermal experiment have satisfied previously mentioned flexural strength as well as shape regularity (twist and cambers) criteria. That is the reason why in this study the lowest TDT value was used as a final criterion for selection of the experiment 8 drying regime as optimal (see **Table 5**, experiment 8).

4. Conclusion

The procedure for setting up the non-isothermal drying regime that is consistent with the theory of moisture migration during drying has demanded to divide the drying process into five segments. For the first time, the choice of isothermal segments specification was achieved in accordance with the theory of moisture migration during drying and with the nature and the properties of the clay raw materials. Duration of the approximately isothermal drying segments was not specified by experience or by trial-and-error method. It was detected from the appropriate isothermal Deff-MR curves. Proposed drying regimes were tested. Dried clay roofing tiles have satisfied all requirements related to the shape regularity and mechanical properties as defined in EN 1304 norm. Finally, experiment 8 was chosen as the optimal drying regime. Semi-industrial trials have shown that the proposed drying regimes obtained from Deff-MR curves can be implemented in real industry system. Namely, the design of the optimal drying curve along with the drying time reduction and higher utilization of the dryer is possible without the fear of generating higher scrap rate. The next step is to apply the presented procedure and to find a way to distinguish the influence of shape factor, forming history and drying parameters on the quality of the dried tiles.

Acknowledgements

This paper was realized under the project ИИИ 45008 which was financed by ministry of education and science of Serbia as well as the company "Potisje Kanjiža".

Author details

Miloš Vasić[1*], Zagorka Radojević[1] and Robert Rekecki[2]

*Address all correspondence to: milos.vasic@institutims.rs

1 Institute for the Testing of Materials, Belgrade, Serbia

2 Potisije Kanjiža, Kanjiža, Serbia

References

[1] Efremov G., Kudra T. Calculation of the effective diffusion coefficients by applying a quasi-stationary equation for drying kinetic. Drying Technology. 2004;22(10):2273–2279.

[2] Vasić M., Radojević Z., Grbavčić Ž. Methods of determination for effective diffusion coefficient during convective drying of clay products. In: Valaškova M., Martynkova S.G., editors. Clay Minerals in nature—their characterization, modification and application. Croatia: Intech; 2012. p. 295–313.

[3] Vasić M., Radojević Z. Calculation of the effective diffusion coefficient. International Journal of Modern Manufacturing Technologies. 2011;3(1):93–98.

[4] Vasić M., Radojević Z., Grbavčić Ž. Calculation of the effective diffusion coefficient during the drying of clay samples. Journal of the Serbian Chemical Society. 2012;77(4): 523–533.

[5] Waccarezza L.M., Lombardi J.L., Chirifle J. Effects on drying rate of food dehydration. Canadian Journal of Chemical Engineering. 1974;52(5):576–579.

[6] Vasić M., Radojević Z., Grbavčić Ž. Determination of the effective diffusion coefficient. Romanian Journal of Material. 2011;42(1):169–176.

[7] Vasić M., Grbavčić Ž., Radojević Z. Determination of the moisture diffusivity coefficient and mathematical modeling of drying. Chemical Engineering and Processing. 2014;76:33–44.

[8] Pinto L.A.A., Tobinaga S. Diffusive model with shrinkage in the thin-layer drying of fish. Drying Technology. 2006;24(4):509–516.

[9] Lopez I.I.R., Espinoza H.R., Lozada P.A., Alvarado A.M.G. Analytical model for moisture diffusivity estimation and drying simulation of shrinkable food products. Journal of Food Engineering. 2012;108:427–435.

[10] Batista M.L., Cezar A.R., Pinto L.A.A. Diffusive model with variable effective diffusivity considering shrinkage in thin layer drying of chitosan. Journal of Food Engineering. 2007;81(1):127–132.

[11] Zagrouba F., Chemki S. Water diffusion coefficient in clay material from drying data. Desalination. 2005;185:491–498.

[12] Vasić M., Grbavčić Ž., Radojević Z. Analysis of moisture transfer during the drying of clay tiles with particular reference to an estimation of the time-dependent effective diffusivity. Drying Technology. 2014;32(7):829–840.

[13] Cranck J. The Mathematics of Diffusion. New York, USA: Oxford University Press; 1975.

[14] Aghbashlo M., Kianmehr M.H., Akhijahani H.S. Influence of drying conditions on the effective moisture diffusivity, energy of activation and energy consumption during the thin-layer drying of berberis fruit (Berberidaceae). Energy Conversion and Management. 2008;49:2865–2871.

[15] Doymaz I. Convective drying kinetics of strawberry. Chemical Engineering and Processing. 2008;47:914–919.

[16] Azzouz S., Guizani A., Jomaa W., Belghith A. Moisture diffusivity and drying kinetic equation of convective drying of grapes. Journal of Food Engineering. 2002;55:323–330.

[17] Vasić M., Radojević Z. Non-isothermal drying process optimisation—drying of clay tiles. In: 3th International Conference Modern Technologies in Industrial Engineering (ModTech2015); 17–20.06.2015; Mamaia, Romania. England: IOP Conf. Series: Materials Science and Engineering 95 (2015) 012025; 2015. p. 1–7. DOI: 10.1088/1757-899X/95/1/012025.

[18] Vasić M., Radojević Z. Setting up the drying regimes based on the theory of moisture migration during drying. In: Dumitru Nedelku, editor. Modern Technologies in Industrial Engineering (ModTech 2016), Book of Abstracts; 15–18.06.2016; Iasi, Romania. Iasi, Romania: Modtech Publishing House; 2016. p. 116.

[19] Kowalski S.J. Thermomechanical approach to shrinking and cracking phenomena in drying. Drying Technology. 2001;19(5):731–765.

[20] Kowalski S. J., Banaszak J. Modeling and Experimental Identification of Cracks in Porous Materials during drying. Drying Technology. 2013;31(12):1388–1399.

[21] Aresnović M., Radojević Z., Stanković S., Lalić Ž., Pezo L.L. What to expect from heavy clay? Ceramic International. 2013;39(2):1667–1675.

[22] Shiming Y. Z., Dengying L. Mechanisms and mathematical model of heat and mass transfer during convective drying of porous materials. Heat Transfer—Asian Research. 1999;28(5):337–351.

[23] Rekecki R., Kuzmann E., Homonnay Z., Ranogajec J. Mossbauer and X-ray study of the firing process for production of improved roofing tiles. Hyperfine Interact. 2013;217(35):27–35.

[24] Rekecki R., Ranogajec J. Design of ceramic microstructures based on waste materials. Processing and Application of Ceramics. 2008;2(2):89–95.

[25] Lalić Ž., Aresenović M., Janaćković Đ., Vasić M., Radojević Z. Influence of increased temperature on clay fast drying process. Romanian Journal of Materials. 2009;39(3): 175–179.